

Surgery with molecular fluorescence imaging using activatable cell-penetrating peptides decreases residual cancer and improves survival

Quyen T. Nguyen^a, Emilia S. Olson^{b,c}, Todd A. Aguilera^{b,c}, Tao Jiang^{b,d}, Miriam Scadeng^e, Lesley G. Ellies^f, and Roger Y. Tsien^{b,d,1}

Departments of ^aSurgery, ^bPharmacology, ^cRadiology, and ^fPathology, ^eMedical Scientist Training Program, and ^dHoward Hughes Medical Institute, University of California at San Diego, La Jolla, CA 92093-0647

Edited* by Robert Langer, Massachusetts Institute of Technology, Cambridge, MA, and approved December 24, 2009 (received for review September 9, 2009)

The completeness of tumor removal during surgery is dependent on the surgeon's ability to differentiate tumor from normal tissue using subjective criteria that are not easily quantifiable. A way to objectively assess tumor margins during surgery in patients would be of great value. We have developed a method to visualize tumors during surgery using activatable cell-penetrating peptides (ACPPs), in which the fluorescently labeled, polycationic cell-penetrating peptide (CPP) is coupled via a cleavable linker to a neutralizing peptide. Upon exposure to proteases characteristic of tumor tissue, the linker is cleaved, dissociating the inhibitory peptide and allowing the CPP to bind to and enter tumor cells. In mice, xenografts stably transfected with green fluorescent protein show colocalization with the Cy5-labeled ACPPs. In the same mouse models, Cy5-labeled free ACPPs and ACPPs conjugated to dendrimers (ACPPDs) delineate the margin between tumor and adjacent tissue, resulting in improved precision of tumor resection. Surgery guided by ACPPD resulted in fewer residual cancer cells left in the animal after surgery as measured by Alu PCR. A single injection of ACPPD dually labeled with Cy5 and gadolinium chelates enabled preoperative whole-body tumor detection by MRI, intraoperative guidance by real-time fluorescence, intraoperative histological analysis of margin status by fluorescence, and postoperative MRI tumor quantification. Animals whose tumors were resected with ACPPD guidance had better long-term tumor-free survival and overall survival than animals whose tumors were resected with traditional bright-field illumination only.

intraoperative fluorescence imaging | molecular navigation | long-term survival | molecular imaging | surgical margin

In 2008, there were 1.5 million new cases of cancer diagnosed in the United States with an estimated healthcare cost of \$89 billion (1). The primary treatment modality for most solid tumors is surgery (2). If the entire tumor is removed with surgery, the patient is potentially cured of cancer. Thus, any improvement in the rate of complete tumor removal in surgery would benefit patients and might produce significant cost savings.

The presence or absence of tumor cells remaining in the surrounding area (the surgical margins) following tumor removal is usually considered of utmost importance in achieving a cure. Positive margins, defined as tumor cells at the cut edge of the surgical specimen, have been associated with increased local recurrence and are a poor prognostic indicator for cancer of the head and neck (3), breast cancer (4, 5), non-small-cell lung cancer (6), colorectal cancer (7), and cancer of the urogenital tract (8, 9). In most situations, the poorer outcome as a result of positive surgical margins is not mitigated by salvage surgery (i.e., re-excision of the positive margin) or by adjuvant chemotherapy and/or radiation (3–9).

There is great interest in approaches that can optimize surgical margins at the initial surgery. For nonpalpable tumors such as some tumors of the breast, tumor localization with the preoperative placement of a physical marker also known as a guide-

wire with mammographic stereotactic guidance or with ultrasound guidance has been used (4). These techniques take advantage of anatomical signatures of the tumor as seen on radiographic imaging or ultrasound to distinguish tumor from adjacent normal tissue. The main disadvantage of these techniques is their limited spatial resolution and the difficulty of translating two-dimensional information to the three-dimensional surgical field.

A more commonly used approach to optimize surgical margins at the initial surgery is through immediate intraoperative (frozen) margin evaluation (4). In this situation, small samples from selected sites of the surgical bed are used to evaluate the presence or absence of residual cancer. Because this process is performed before wound closure or reconstruction, it extends anesthesia-related risks for the patient, is time-consuming and labor intensive, and increases cost to the healthcare system. Furthermore, there are instances in which the intraoperative analysis of surgical margins was thought to be free of tumor, but pathological analysis at a later time reveals the presence of cancer at the margins. These patients must choose to either undergo a second surgery where the same uncertainty of margin status applies or opt for a less optimal treatment modality. In this study, we investigated whether tumor margins could be visualized more objectively during surgery using activatable cell-penetrating peptides (ACPPs) (10). We compared residual tumor cells at the surgical bed and tumor-free survival following surgery with and without ACPP molecular guidance.

Results

Tumor Imaging with Cy5-Labeled Free ACPP. To test whether ACPPs are taken up differentially between tumor and normal tissue, we examined four tumor models: isografts derived from spontaneous mammary adenocarcinoma tumors in transgenic mice (line 8119, MMTV-PyMT) (11, 12), the murine melanoma cell line B16F10 transplanted into immune-competent mice, and human cancer cell lines (MDA-MB 435 melanoma and HT1080 fibrosarcoma) xenografted into nude mice. Both unadorned ACPPs not conjugated to macromolecules [free ACPPs (12)] and ACPPs conjugated to a generation 5 poly(amidoamine) dendrimer [ACPPs conjugated to dendrimers (ACPPDs) (13)] were separately injected i.v. and imaged by the deep red fluorescence of their Cy5 labels after sufficient time for elimination from normal tissues

Author contributions: Q.T.N., E.S.O., T.A.A., and R.Y.T. designed research; Q.T.N., E.S.O., T.A.A., and M.S. performed research; T.J. and L.G.E. contributed new reagents/analytic tools; Q.T.N., E.S.O., T.A.A., and R.Y.T. analyzed data; and Q.T.N. and E.S.O. wrote the paper.

Conflict of interest statement: Q.T.N., E.S.O., T.A.A., T.J., and R.Y.T. have signed a scientific advisory agreement with a company founded to develop the technology described in this article.

*This Direct Submission article had a prearranged editor.

Freely available online through the PNAS open access option.

¹To whom correspondence should be addressed. E-mail: rtsien@ucsd.edu.

This article contains supporting information online at www.pnas.org/cgi/content/full/0910261107/DCSupplemental.

lacking protease activity (typically 6 h for free ACPPs and 48 h for ACPPDs). All tumors retained the Cy5-labeled free ACPP and ACPPD to a greater extent than normal tissues or tissue treated with protease-resistant controls (12, 13). Furthermore, tumor-to-normal tissue ratios from all tumor types were greater with ACPPD compared to free ACPP (Table 1).

ACPPs and ACPPDs Delineate Tumor at the Margin of Resection. To assess the ability of ACPPs to delineate the margin between normal and tumor tissue, we injected nude mice xenografted with the green fluorescent protein (GFP)-transfected cell line MDA-MB-435 i.v. with Cy5-labeled free ACPP before surgical excision of tumors. We found that, if the tumors had infiltrated into surrounding tissue, free-ACPP guidance resulted in the ability to visualize areas of tumors that are not apparent with white light [either because they are buried beneath other tissue (Fig. 1) or the appearance of the tumor is not easily distinguishable from surrounding normal tissue].

We compared free ACPPs and ACPPDs for their tumor-to-background visual fluorescence contrast and ease of use during in vivo surgery ($n = 16$ each condition; Fig. 2). For the same amount of fluorophore injected, ACPPD gave much higher absolute tumor fluorescence and tumor-to-background fluorescence contrast than free ACPPs (Fig. 2). Conjugation to macromolecular carriers such as dendrimers greatly reduces uptake by skin, cartilage, and kidney (13). We did note limited fluorescence uptake for both free ACPPs and ACPPDs into lymph nodes as well as fatty tissue that is not dependent on the presence of cancer cells. This is likely due to uptake by macrophages, whose presence is abundant in both of these tissues.

Residual Tumor Cell Quantification with Alu PCR. To quantify the efficacy of MDA-MB 435 tumor excision with free-ACPP and ACPPD guidance, we used Alu PCR (14) to measure residual human (cancer) cells remaining in the tumor bed after surgical excision. The quantification of human Alu sequences has been shown to be able to detect the equivalent of one human tumor cell in 1×10^6 murine cells (14). Tumor margins can thus be detected sensitively by using human Alu PCR. We found that ACPPD guidance resulted in 10-fold fewer residual tumor cells at the surgical site (i.e., 90% reduction of residual cancer cells) [$\log(\text{DNA}) = 3.67 \pm 0.47, n = 10$] compared to unguided surgery done using standard technique [$\log(\text{DNA}) = 4.63 \pm 0.82, n = 10$; two-

tailed Student's t test, $P = 0.005$; Fig. 3]. In contrast, surgery using GFP fluorescence inherent to the cancer cells to guide excision [$\log(\text{DNA}) = 4.0 \pm 1.4, n = 7$] or surgery with free ACPP [$\log(\text{DNA}) = 4.67 \pm 0.33, n = 6$] did not show improved efficacy compared to standard unguided surgery [$\log(\text{DNA}) = 4.63 \pm 0.82, n = 10$; $P = 0.26$ and 0.91 , respectively]. We hypothesize that cells within the xenografts lose GFP expression due to selective pressures, and thus some cancer cells may be missed during GFP fluorescence survey of the tumor bed, resulting in incomplete resection of the tumor. In addition, because GFP excitation and emission are absorbed by tissue and hemoglobin in the living animal, tumors that are not on the surface of the surgical bed may be missed (Fig. 1). The lack of improved cancer removal efficacy with free-ACPP guidance likely reflects the lower free-ACPP uptake by tumor tissue and thus reduced contrast of the free ACPP between tumor and adjacent normal tissue (2.45-fold) compared to ACPPDs (4.46-fold). Consistent with this observation, there is a significant reduction of residual tumor cells using ACPPD guidance compared to free-ACPP guidance (two-tailed Student's t test, $P = 0.0005$) (Fig. 3).

Histological Analysis of Surgical Specimens Derived from ACPPD-Guided Surgery. To quantify the correlation between high fluorescence uptake and presence of malignant cells, we performed histological analysis on individual ACPPD-guided resected margins from B16F10 isografts. We found that the ACPPD probe has a specificity rate of 93% (i.e., hematoxylin/eosin histological analysis showed malignant cells in 14 of 15 specimens obtained from ACPPD-guided excision, a representative section of which is shown in Fig. 4).

Depth of Detection for Tumor Labeled with Cy5-ACPPD. To quantify the depth of tumor detection, 1-mm³ tumor fragments derived from animals treated with Cy5-ACPPD were placed underneath muscle flaps of increasing thickness (0.5–3 mm). Fluorescence of the covered tumor specimens and background were measured by imaging, and the ratio was calculated. The tumor size was chosen to approximate the size of tumor specimens that would be clinically possible to resect in surgery with human patients. We found that tumor-to-background contrast decreased with increasing thickness of overlying tissue with a maximal detection depth of around 2.5 mm (Fig. S1).

ACPPD Guidance for Surgery by both Fluorescence and MRI. In addition to fluorescence imaging, ACPPD imaging with MRI can also be used to evaluate the completeness of tumor surgery. Fig. 5 shows nude mice with HT1080 (Fig. 5A–D) or MDA-MB 435 (Fig. 5E–H) xenografts after i.v. injection with ACPPD bearing both Cy5 and gadolinium-1,4,7,10-tetraazacyclododecane-1,4,7,10-tetraacetic acid (DOTA). Before resection, the tumors were easily visible both by T₁-weighted MRI (Fig. 5A and E) and fluorescence (Fig. 5B and F). In some animals, postoperative MRI (Fig. 5C) showed residual ACPPD just beyond the site of resection. Histological analysis of tissue (Fig. 5D) obtained from these areas postmortem using ACPPD-guided fluorescence imaging confirmed the presence of cancer cells. Other resections were more complete and showed no detectable residual tumor by either fluorescence (Fig. 5G) or MRI (Fig. 5H). The volume of MDA-MB 435 xenografts was quantified by using the magnetic resonance (MR) images before and after fluorescence ACPPD-guided excision of the tumor in a blinded fashion. We found that surgery with Cy5-ACPPD fluorescence guidance resulted in approximately a fivefold reduction of residual tumor on the basis of the volumetric analysis of the MRI scan compared to standard unguided surgery [$15.8 \pm 7.8 \text{ mm}^3 (n = 2)$ vs. $3.3 \pm 2.7 \text{ mm}^3 (n = 2)$]. Although this result did not reach statistical significance (Student's t test, one-tailed, $P = 0.08$) likely because of the small sample size, it is consistent with the above result showing

Table 1. Standardized uptake values comparing free ACPP to ACPPD for different tumor models

	Free ACPP	ACPPD
MDA-MB 435		
Tumor	$0.71 \pm 0.05 (n = 3)$	$1.065 \pm 0.55 (n = 3)$
Muscle	$0.29 \pm 0.068 (n = 3)$	$0.238 \pm 0.007 (n = 3)$
Ratio	$2.45 (P = 0.0004)$	$4.46 (P = 0.031)$
HT1080		
Tumor	$0.55 \pm 0.28 (n = 4)^*$	$1.8 \pm 0.6 (n = 8)^\dagger$
Muscle	$0.11 \pm 0.08 (n = 4)$	$0.21 \pm 0.07 (n = 8)$
Ratio	$5.25 (P = 0.022)$	$8.6 (P = 0.0009)$
8119		
Tumor	$0.39 \pm 0.12 (n = 5)^*$	$2.191 \pm 0.743 (n = 3)$
Muscle	$0.11 \pm 0.06 (n = 5)$	$0.166 \pm 0.023 (n = 3)$
Ratio	$3.5 (P = 0.006)$	$13.2 (P = 0.004)$
B16F10		
Tumor	$0.24 \pm 0.06 (n = 4)^*$	$1.069 \pm 0.575 (n = 3)$
Muscle	$0.10 \pm 0.03 (n = 3)$	$0.191 \pm 0.014 (n = 3)$
Ratio	$2.4 (P = 0.014)$	$5.6 (P = 0.028)$

*ref. (12).

†ref. (13).

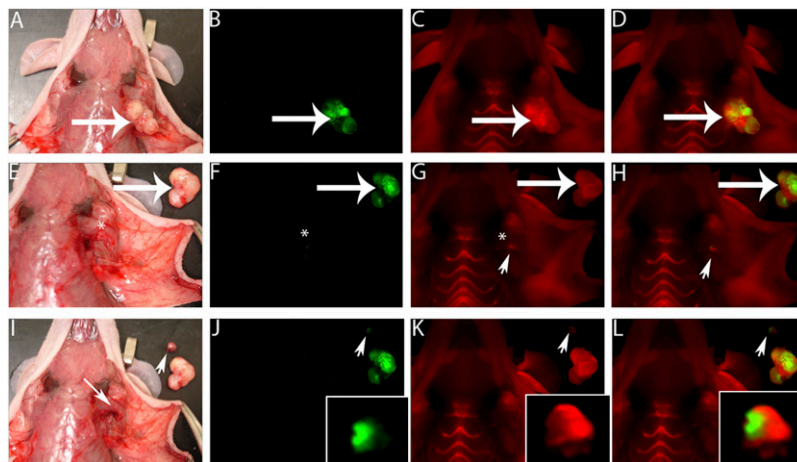


Fig. 1. ACPPs delineate tumor at the margin of resection. (A) White light image of a MDA-MB 435 xenograft following skin incision and tumor (large arrow) exposure. (B) Fluorescence image of GFP-labeled tumor cells from the same animal as in A. (C) Fluorescence image 6 h following i.v. administration of Cy5-labeled free ACPP showing increased uptake by the tumor (large arrow) compared to surrounding tissue. (D) Overlay fluorescence image showing colocalization of the Cy5 free ACPP with the GFP-labeled tumor. Following gross tumor excision by standard (unguided) technique, the tumor bed (*) seen with white light (E) appears to be free of tumor [the excised tumor (large arrow) has been laid next to the mouse]. (F) Fluorescence imaging of the GFP signal in the tumor bed appears to confirm complete tumor excision (*). However, imaging of the Cy5 signal (G and H) demonstrates a residual fluorescence signal (arrowhead) in surrounding remaining tissue (i.e., surgical margin). Using the Cy5 fluorescence to guide exploration (G and H), a small piece of residual tumor (arrowhead) is identified buried underneath the pectoralis muscle (I, small arrow). Interestingly, once the tumor has been dissected out from its buried position under the pectoralis muscle, the GFP signal (J, arrowhead) confirming the presence of tumor cells can be visualized along with the Cy5 free ACPP signal (K and L). (J–L, insets) The excised tumor magnified and brightened 5 \times .

reduced residual tumor cells following ACPPD-guided surgery by Alu PCR quantification (Fig. 3).

Improved Tumor-Free Survival with ACPPD-Guided Surgery. To test whether tumor recurrence is affected when surgery is done with ACPPD guidance, we injected Cy5-labeled ACPPD into immunocompetent mice grafted with syngeneic cells derived either from spontaneous tumors in transgenic mice (line 8119, MMTV-PyMT) or from the melanoma cell line (B16F10). When the tumors infiltrated into surrounding tissue, we found that mice

whose tumors were excised with ACPPD guidance showed improved tumor-free survival compared to mice whose tumors were excised without ACPPD guidance (Fig. 6). In mice isografted with the melanoma cell line B16F10, surgery with ACPPD guidance resulted in a doubling of improved tumor-free survival in the short term (40% compared to 20% at 8 weeks following surgery) and a 50% improvement of tumor-free survival at longer times (33% compared to 22% at 24 weeks; Wilcoxon test, $P = 0.05$) (Fig. 6A). In mice isografted with the transgenic 8119 breast-cancer cell line, surgery with ACPPD guidance resulted in a fivefold improvement of long-term (24 weeks) tumor-free survival compared to standard surgery (50% compared to 10% at 20 weeks following surgery; Wilcoxon

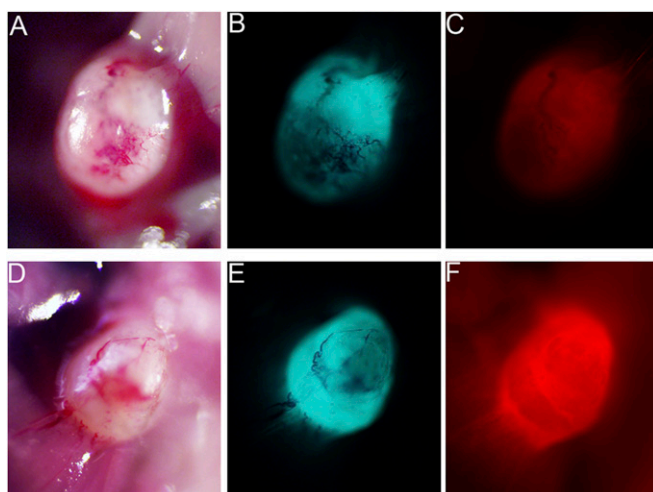


Fig. 2. Comparing free ACPP and ACPPD for fluorescence imaging guidance. White light (A and D) and fluorescence images showing GFP-labeled MDA-MB 435 xenografts (B and E) from mice that were treated with Cy5-labeled free ACPP (C) and ACPPD (F). In tumors of comparable size, treatment with the free ACPP (C) or ACPPD (F) resulted in tumor-specific fluorescence uptake. There is a higher tumor-to-background fluorescence contrast for the ACPPD compared to free ACPPs and a higher absolute tumor fluorescence for ACPPDs when normalized to Cy5 fluorescence injected. Cy5 fluorescence images (C and F) were adjusted for total nanomoles of Cy5 injected per animal.

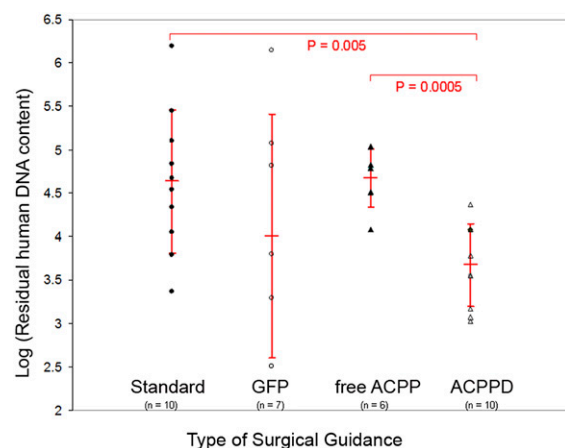


Fig. 3. ACPPD guidance results in fewer residual tumor cells quantified by Alu PCR. Scatter plot showing residual human DNA content (i.e., tumor cells) for each type of surgery (standard surgery with no molecular guidance, GFP guidance, Cy5 free ACPP guidance, Cy5-ACPPD guidance). Vertical bar for each type of surgical condition shows the log of the mean and the standard deviation of human cell number that remained following surgery from the cohort of mice. There is significantly fewer residual human DNA content for surgery with ACPPD guidance compared to any other surgical conditions.

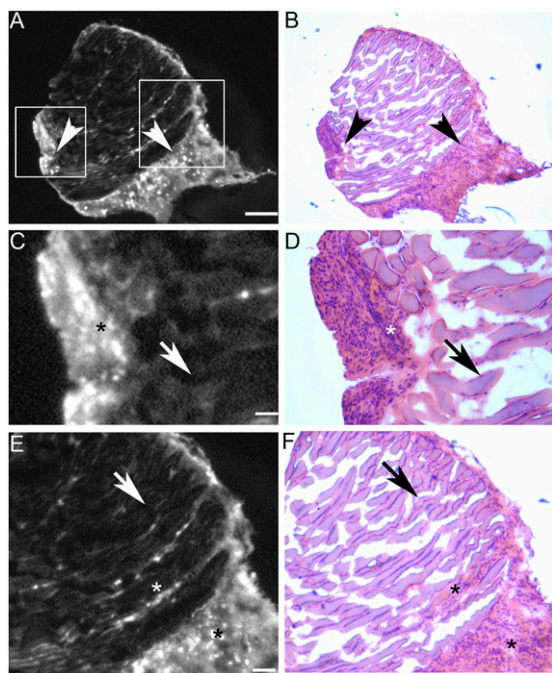


Fig. 4. Histological analysis of surgical specimens derived from ACPPD-guided surgery. Photomicrographs showing a representative specimen from the B16F10 isograft model that was excised with fluorescently labeled ACPPD guidance. (A) Low-power Cy5 fluorescence showing positive ACPPD uptake (arrowheads). (B) The same section as in A stained with H&E, confirming the presence of malignant cells in regions that show increased fluorescence uptake (arrowheads). (C and E) Enlarged fluorescence images from the boxed areas in A, showing the demarcation between high (*) and low (arrows) fluorescence uptake. (D and F) Histological (H and E) analysis of C and E, showing that the areas of high fluorescence uptake correspond to malignant cells (*). (Scale bar in A and B: 0.5 mm; C and D: 0.1 mm; E and F: 0.25 mm.)

test, $P = 0.03$) (Fig. 6B). The Wilcoxon test used in the analysis is a variation of the log-rank test with emphasis on the information at the beginning of the survival curve where the number at risk is large, allowing early failures to receive more weight than later failures. We believe this is a valid analysis as tumor recurrence tended to occur early on in the postoperative period (all tumor recurrences occurred within the first 8 weeks for both animal models).

Discussion

We have developed an objective means of visualizing the delineation between normal tissue and invasive tumor *in vivo* for use during surgery by using activatable cell-penetrating peptides. We show that in mice, imaging fluorescently labeled free ACPP and ACPPD during surgery can provide visual guidance to show tumor that is either not readily distinguishable from adjacent normal tissue with white light or that is obscured from view by overlying tissue. In the same mouse models, we found that ACPPD is superior to free ACPP for visualizing tumor tissue during surgery in living mice. Using Alu PCR, we found on average 90% fewer residual cancer cells following surgery with ACPPD-based fluorescence guidance compared to standard surgery. We show that fluorescently labeled ACPPD can be used to guide excision of residual tumor with 93% specificity. We believe that ACPPD uptake by macrophages accounts for the observed fluorescence at the margin of resection in the absence of tumor cells in the remaining sample. In the accompanying article by Olson et al. (13), we show that regions of inflammation and F4/80-positive macrophages within the tumor margin are often particularly high in ACPPD uptake. Thus, we think that prudent oncologic resection should include these regions, even

though they are not composed entirely of tumor and much of the fluorescence is contributed by phagocytes.

Tumor volume measurements with MRI imaging using the dually labeled ACPPD (Cy5 and gadolinium-DOTA) showed that residual tumor volume is reduced by fivefold with ACPPD guidance compared to standard unguided surgery. Immune-competent mice with syngeneic tumor transplants excised with ACPPD guidance showed improved long-term tumor-free survival compared to mice whose tumors were excised without ACPPD guidance. To account for bias in performing ACPPD-guided versus standard surgery, all animals regardless of whether or not they were going to have fluorescence-guided surgery underwent standard surgical resection of their tumors under microscopic visualization. The first-pass surgery (no fluorescence guidance) was done with the operating surgeon semiblinded to whether or not the animals were eventually going to undergo fluorescence-guided surgery. Only animals that had satisfactory outcome from the first-pass surgery (i.e., adequate muscular and neural function) were then allowed to either recover from surgery or undergo further fluorescence-guided surgery.

ACPPDs can be used at multiple stages in the evaluation and treatment of cancer. The dual modality (MR and fluorescence) ACPPDs should allow preoperative staging by oncologists and radiologists, particularly for cancers such as prostate where invasion of a capsule is important (9), preventing surgery on patients who are nonoperative candidates. For patients who do undergo surgery, the anatomical and biochemical information given by the dual-labeled ACPPD should be useful for surgeons in planning complex surgical procedures. During surgery, tight binding of ACPPDs to the site of cleavage provides localized information regarding tumor biology that not only allows the surgeon to focus on the most invasive areas of tumor growth with intraoperative fluorescence imaging, but also allows the pathologist to do the same with intraoperative histology. Following surgery, the dual probe allows further evaluation for completeness of tumor removal with a second MRI. With standard gadolinium MRI, postoperative changes tend to enable increased untargeted gadolinium uptake that cannot be differentiated from residual tumor, unless the MR scan is performed within hours after surgery (which may not be possible for all patients depending on scanner availability and patient stability after surgery). Therefore, standard gadolinium-based MRI has limited utility for the evaluation of residual tumor. However, because the ACPPD dual probe is administered before surgery and should have cleared from circulation, contrast agent accumulation seen in the postoperative scan should be attributable to preoperative uptake rather than postoperative tissue damage.

From a molecular-imaging perspective, ACPPDs have several advantages over other targeted fluorescent probes previously described in the literature for use in a surgical system (15–25). Molecular fluorescence-guided surgery demands that a given probe (a), works for a wide variety of tumor types (b), offers ample signal with low background (c), binds tightly to the tumor, and (d), is not affected by the physical trauma of surgery. Although antibody approaches to fluorescence-guided surgery are attractive for individual tumor types that express unique surface markers such as colon (15), pancreas (16), or ovary (17), they are often not applicable to all tumor types. Most tumor antigens such as CEA and CA19-9 have no known etiological function, as demonstrated by their frequent elimination during passage in culture. We prefer targets such as MMP-2 and MMP-9 that play widespread and well-documented roles in tumor progression and metastasis. At the other end of the spectrum are probes that access tumors via their leaky vasculature (18). These probes are applicable to a wide range of tumors but are limited by contrast and nonspecificity. Other options that offer similar fluorescence contrast to ACPPD are the dequenching probes designed by Weissleder's group (19, 20), peptide-based probes that target an abundant ligand such as

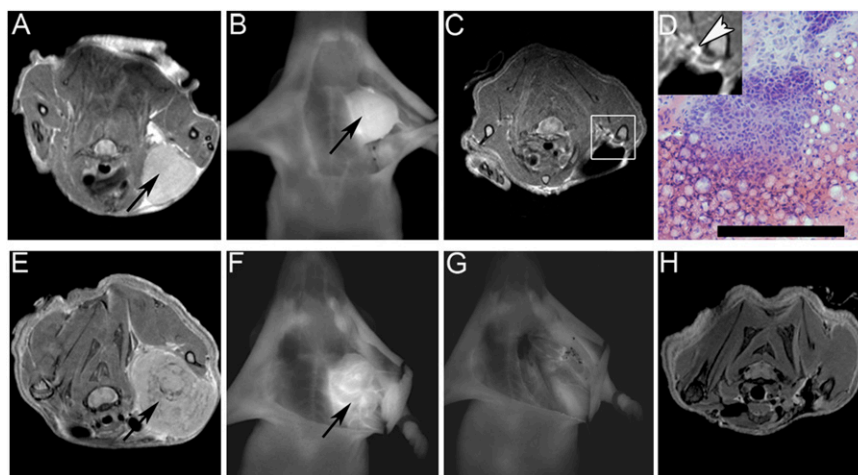


Fig. 5. Dual-Labeled ACPDD. (A–D) Example of HT1080 xenograft treated with ACPDD dually labeled with gadolinium and Cy5. Preoperative MR image of mouse showing contrast uptake in tumor (A, black arrow). Following skin incision and retraction, the tumor (black arrow) on the left chest wall was visible with Cy5 fluorescence (B). Following initial surgery, repeat MRI (C) showed a small area of tissue with increased gadolinium uptake (D inset, white arrowhead). This area of tissue was identified using fluorescence imaging at a second surgery. Histological analysis of this tissue confirmed the presence of cancer cells (D). (Scale bar: 100 μ m). (E–H) Example of MDA-MB 435 xenograft treated with ACPDD dually labeled with gadolinium and Cy5. Preoperative MR image of mouse showing contrast uptake in tumor (E, black arrow). Following skin incision and retraction, the tumor (black arrow) on the left chest wall was visible with Cy5 fluorescence (F). Tumor was resected using ACPDD–Cy5 imaging guidance until all visible fluorescence was completely removed (G). Repeat MR imaging following surgery showed complete removal of all tumor (H).

the $\alpha\beta3$ integrin (21), or 5-aminolevulinic acid (5-ALA) and derivatives, which get converted to fluorescent protoporphyrin IX in many tumors (22, 23). All of these alternatives are limited to fluorescence readout, whereas ACPDD also allows MRI, whose noninvasive depth penetration and tomographic accuracy are ideally complementary to the high spatial resolution, real-time capability, and surgical compatibility of fluorescence. The only reports of postoperative survival were with 5-ALA, which improved 6-month progression-free survival but not long-term survival after resection of malignant gliomas (24), admittedly a very challenging application. Concerns with 5-ALA include the need to excite protoporphyrin IX with violet light, which has very poor penetration through tissue, and the likelihood that tumor cells do not need to up-regulate protoporphyrin IX biosynthesis to remain malignant. ACPDDs exploit both enzymatically amplified adhesion and enhanced permeability and retention due to leaky vasculature and thereby highlight the invasive, protease-producing edge of tumors without sacrificing the ability to see the less proteolytically active core.

In conclusion, we offer evidence that fluorescence and gadolinium-labeled ACPDDs provide molecular navigation to aid margin evaluation during complex surgical resection of large and invasive tumors, thereby decreasing the amount of tumor left behind and increasing tumor-free survival as well as overall survival. Although we used an

open operative technique, this technology should be well suited to laparoscopic and robotic surgery where the lack of haptic (tactile) feedback (26) could benefit from extra visual cues about the tumor margin such as those provided by ACPDDs.

Materials and Methods

Animals. Xenografts with HT1080 human fibrosarcoma cells (American Type Culture Collection) or MDA-MB 435 human melanoma cells (obtained from David Tarin, University of California, San Diego) were generated by Explora Biosciences. Syngeneic grafts were generated in the lab with 8119 murine mammary adenocarcinoma cells (12) and B16F10 murine melanoma cells obtained from Robert Hoffman and AntiCancer. A total of 1×10^6 cells (either 8119 or B16F10) were injected intramuscularly into the left flank of albino C57BL/6 mice (stock 00058; Jackson Labs). Tumor isografts were monitored until tumor size was ≈ 1 cm in largest diameter (≈ 7 –10 days). All animal procedures were approved by the University of California at San Diego's institutional animal care and use committee.

Fluorescent Optical Imaging. Fluorescent optical imaging were performed with a fluorescent dissecting microscope (Lumar, Zeiss [GFP: exposure times 0.5–1 s, ex470/40 nm; em525/50 nm; Cy5: exposure times 0.5–1 s, ex620/60 nm; em700/75 nm]) with the OV100 small animal imaging system (Olympus [GFP: exposure times 0.5–1 s, ex475/40; em 530/50; Cy5: exposure times 1.5–3 s, ex620/60 nm; em700/75 nm] or with the Maestro small animal imaging system (Cy5, exposure times 200 ms–3 s, ex640/48, em700 nm; CRI). (Animals were imaged at 1 s and at 3 s using a Maestro spectral deconvolution imager (em700 nm) using a 640/48 excitation filter (CRI).

Fluorescence Uptake. Standardized uptake values (SUV) were measured as described in Aguilera et al. (11) and Olson et al. (12, 13). Briefly, 30-mg tissues were homogenized and heated in SDS buffer, frozen, and then imaged by fluorescence. SUV [(mol/g tissue)/(mol injected/weight of the animal)] values were determined by comparing experimental fluorescence to standard curves derived by peptide-spiked tissue processed similarly.

Survival Surgery. Survival surgeries were performed on isografts with 8119 cells or B16F10 cells generated as detailed above. Animals were anesthetized with 80 mg/kg ketamine and 40 mg/kg midazolam. Following hair removal with depilatory cream, animals were prepped and draped in sterile fashion. Following skin incision over the tumor, skin flaps were developed and retracted. Tumor excision was performed with microsurgical instrumentations under a dissecting microscope (Lumar, Zeiss) with white light illumination. Hemostasis was achieved with handheld cautery (Accu-Temp, Medtronic). Following complete tumor removal as assessed by white light

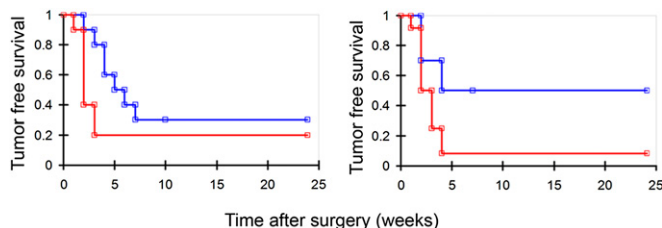


Fig. 6. Kaplan–Meier survival curve. Tumor-free survival after surgery versus time (weeks) for (left) B16F10 ($n = 10$ for ACPDD guidance, $n = 10$ for standard surgery, Wilcoxon test, $P = 0.05$) or (right) 8119 ($n = 10$ for ACPDD guidance, $n = 12$ for standard surgery, Wilcoxon test, $P = 0.03$) isografts showing improved long-term tumor-free survival with Cy5–ACPDD guidance (blue) compared to standard surgery (red) without ACPDD guidance.

illumination, animals were placed into either Cy5 fluorescence guidance arm surgery or standard surgery with no molecular guidance arm. Standard surgery is defined as surgery with white light illumination under microscopic visualization to remove the entire ascertainable tumor. The mice were included in the analysis for tumor-free survival only if they had achieved tumor-free status as ascertained clinically by the surgeon at completion of surgery. Animals that were in the ACPD guidance arm were injected with Cy5-labeled ACPD (2 nmol) 48 h before the beginning of tumor excision. In an attempt to account for bias during the initial surgery, the operating surgeon was semiblinded as to the treatment arms that the animals would receive after the initial tumor removal. Semiblinding meant that the operating surgeon made a conscious effort to not identify animals by which treatment arms they were assigned. However, because it was occasionally the same person who treated the animals with ACPDs via tail-vein injections as the person who did the tumor resection, animal identification via visual characteristics of individual animals was sometimes unavoidable.

Following complete tumor excision as assessed by white light illumination, the surgical field was then assessed through the dissecting scope with excitation and emission parameters for Cy5. Images of the fluorescence signal were displayed on an adjacent monitor and all Cy5-positive tissue foci were excised. Following completion of tumor removal either with or without fluorescence guidance, skin incisions were repaired with interrupted simple sutures (6-0 silk; Ethicon), and animals were returned to their cages to recover from the anesthesia.

All animals deemed clinically tumor-free at completion of surgery (both standard and ACPD-guided) were monitored for tumor recurrence. Recurrences observed were local tumor recurrences confirmed by biopsy. We did not observe any evidence of metastatic disease in any animals. Animals were examined for tumor recurrence three times per week. All animals were killed regardless of the presence or absence of tumor recurrence at 6 months following surgery. All animal procedures were approved by the University of California at San Diego's institutional animal care and use committee.

Quantification of Residual Tumor Cells. Animals used for quantification of residual tumor cells after surgery were performed on xenograft of MDA-MB 435 cells generated as detailed above. Animals were anesthetized with 80 mg/kg ketamine and 40 mg/kg midazolam. Following skin incision and retraction, tumors were removed with microsurgical technique using a dissecting micro-

scope (Lumar; Zeiss). Fluorescence guidance of tumor excision was performed as detailed above for the survival studies with GFP, free ACPD (10 nmol; 6 h before surgery), or ACPD (2 nmol; 48 h before surgery). For animals in the GFP guidance arm, the surgical field was assessed through the dissecting scope with excitation and emission parameters for GFP. Images of the fluorescence signal were displayed on an adjacent monitor and all GFP-positive tissue foci were excised. Treatment of the animals in the free-ACPD and ACPD arms were performed as in the survival surgeries described above. Following completion of tumor resection, the remaining surgical bed was resected with at least a 5-mm margin in all contiguous dimensions and analyzed for Alu sequences. Alu PCR analysis of the remaining surgical bed for residual tumor cells was performed as previously described by the Quigley lab (14). Because the PCR assay measures the number of cycles necessary to reach detectability, which is proportional to the log of the amount of source DNA, residual tumor DNA is represented in log units.

Fluorescence and MR Imaging with Dual-Labeled ACPD. HT1080 and MDA-MB 435 xenografts were generated as described above and injected with dual-labeled ACPD. Preoperative MR imaging of the mice was performed as previously described (12). Mice were then anesthetized and tumor removed with fluorescence guidance as described above. Following complete tumor removal, mice were brought to the MR imaging suite and postoperative MR scans were obtained. Tumor volume quantification was performed on MDA-MB 435 mice. Tumor volume was quantified off T₁- and T₂-weighted MR images three-dimensionally by hand using Amira software (Mercury) in a blinded fashion by separate personnel.

ACKNOWLEDGMENTS. The authors thank Dr. David Tarin (UCSD) for his generous gift of the GFP-transfected MDA-MB435 cell line and Anticancer Inc. for their generous gift of the B16F10 cell line. The authors thank Dr. James Quigley and Erin Conn for their help in performing the Alu PCR analysis. The authors also thank Ms. Perla Arcaira for performing tissue processing for SUVs and for generating the tumor xenograft/isografts and Mr. Paul Steinbach for his assistance with measuring tumor depth of detection. This work was supported by the Howard Hughes Medical Institute, an Era of Hope Innovator Award from the US Army Department of Defense (Grant W81XWH-05-1-0183 to R.Y.T), and the National Institutes of Health (Grant NIBIB-K08 EB008122 to Q.T.N).

- Ries LAG, et al. (2008). SEER Cancer Statistics Review, 1975–2005, (National Cancer Institute, Bethesda, MD), <http://seer.cancer.gov/csr/1975-2005/>, based on November 2007 SEER data submission, posted to the SEER web site.
- Pattern of Care Studies/Quality of Care Studies (2008). SEER Cancer Statistics Review, 1975–2005, (National Cancer Institute, Bethesda, MD), <http://seer.cancer.gov/csr/1975-2005/>, based on November 2007 SEER data submission, posted to the SEER web site.
- Haque R, Contreras R, McNicoll MP, Eckberg EC, Petitti DB (2006). Surgical margins and survival after head and neck cancer surgery. *BMC Ear Nose Throat Disord* 6:2.
- Singletary SE (2002) Surgical margins in patients with early-stage breast cancer treated with breast conservation therapy. *Am J Surg* 184:383–393.
- Meric F, et al. (2003) Positive surgical margins and ipsilateral breast tumor recurrence predict disease-specific survival after breast-conserving therapy. *Cancer* 97:926–933.
- Snijder RJ, Brutel de la Rivière A, Elbers HJJ, van den Bosch JMM (1998) Survival in resected stage I lung cancer with residual tumor at the bronchial resection margin. *Ann Thorac Surg* 65:212–216.
- Nagtegaal ID, Quirke P (2008) What is the role for the circumferential margin in the modern treatment of rectal cancer? *J Clin Oncol* 26:303–312.
- Dotan ZA, et al. (2007) Positive surgical margins in soft tissue following radical cystectomy for bladder cancer and cancer specific survival. *J Urol* 178:2308–2312; discussion 2313.
- Wieder JA, Soloway MS (1998) Incidence, etiology, location, prevention and treatment of positive surgical margins after radical prostatectomy for prostate cancer. *J Urol* 160:299–315.
- Jiang T, et al. (2004) Tumor imaging by means of proteolytic activation of cell-penetrating peptides. *Proc Natl Acad Sci USA* 101:17867–17872.
- Aguilera TA, Olson ES, Timmers MM, Jiang T, Tsiens RY (2009) Systemic *in vivo* distribution of activatable cell penetrating peptides is superior to cell penetrating peptides. *Integr Biol (Camb)* 1:371–381.
- Olson ES, et al. (2009) *In vivo* characterization of activatable cell penetrating peptides for targeting protease activity in cancer. *Integr Biol (Camb)* 1:382–393.
- Olson ES, et al. (2010) Activatable cell penetrating peptides linked to nanoparticles as dual probes for *in vivo* fluorescence and MR imaging of proteases. *Proc Natl Acad Sci USA* 107:4311–4316.
- Zijlstra A, et al. (2002) A quantitative analysis of rate-limiting steps in the metastatic cascade using human-specific real-time polymerase chain reaction. *Cancer Res* 62: 7083–7092.
- Kaushal S, et al. (2008) Fluorophore-conjugated anti-CEA antibody for the intraoperative imaging of pancreatic and colorectal cancer. *J Gastrointest Surg* 12:1938–1950.
- McElroy M, et al. (2008) Imaging of primary and metastatic pancreatic cancer using a fluorophore-conjugated anti-CA19-9 antibody for surgical navigation. *World J Surg* 32:1057–1066.
- Longmire M, Kosaka N, Ogawa M, Choyke PL, Kobayashi H (2009) Multicolor *in vivo* targeted imaging to guide real-time surgery of HER2-positive micrometastases in a two-tumor coincident model of ovarian cancer. *Cancer Sci* 100:1099–1104.
- Kremer P, et al. (2009) Intraoperative fluorescence staining of malignant brain tumors using 5-aminofluorescein-labeled albumin. *Neurosurgery* 64 (Suppl 3):53–60; discussion 60–61.
- Bremer C, Bredow S, Mahmood U, Weissleder R, Tung CH (2001) Optical imaging of matrix metalloproteinase-2 activity in tumors: Feasibility study in a mouse model. *Radiology* 221:523–529.
- Bremer C, Tung CH, Bogdanov A, Jr, Weissleder R (2002) Imaging of differential protease expression in breast cancers for detection of aggressive tumor phenotypes. *Radiology* 222:814–818.
- Jin ZH, et al. (2007) *In vivo* optical imaging of integrin alphaV-beta3 in mice using multivalent or monovalent cRGD targeting vectors. *Mol Cancer* 6:41.
- Krammer B, Plaetzer K (2008) ALA and its clinical impact, from bench to bedside. *Photochem Photobiol Sci* 7:283–289.
- Tonn JC, Stummer W (2008) Fluorescence-guided resection of malignant gliomas using 5-aminolevulinic acid: Practical use, risks, and pitfalls. *Clin Neurosurg* 55:20–26.
- Stummer W, et al. (2006) Fluorescence-guided surgery with 5-aminolevulinic acid for resection of malignant glioma: A randomised controlled multicentre phase III trial. *Lancet Oncol* 7:392–401.
- Frangioni JV (2008) New technologies for human cancer imaging. *J Clin Oncol* 26: 4012–4021.
- Hu JC, Wang Q, Pashos CL, Lipsitz SR, Keating NL (2008) Utilization and outcomes of minimally invasive radical prostatectomy. *J Clin Oncol* 26:2278–2284.